Structure determination of selenomethionyl S-adenosylhomocysteine hydrolase using data at a single wavelength

Mary A. Turner[1], Chong-Sheng Yuan[2,3], Ronald T. Borchardt[2], Michael S. Hershfield[4], G. David Smith[5,6] and P. Lynne Howell[1,7]

S-Adenosylhomocysteine (AdoHcy) hydrolase regulates all adenosylmethionine-(AdoMet) dependent transmethylations by hydrolyzing the potent feedback inhibitor AdoHcy to homocysteine and adenosine. The crystallographic structure determination of a selenomethionyl-incorporated AdoHcy hydrolase inhibitor complex was accomplished using single wavelength anomalous diffraction data and the direct methods program, *Snb* v2.0, which produced the positions of all 30 crystallographically distinct selenium atoms. The mode of enzyme–cofactor binding is unique, requiring interactions from two protein monomers. An unusual dual role for a catalytic water molecule in the active site is revealed in the complex with the adenosine analog 2'-hydroxy, 3'-ketocyclopent-4'-enyladenine.

Donation of an activated methyl group from S-adenosylmethionine (AdoMet) to numerous acceptors, ranging from low molecular weight neurotransmitters and hormones to all classes of macromolecules affects diverse aspects of metabolism, gene regulation, and cellular function[1]. The product of these methylation reactions is S-adenosylhomocysteine (AdoHcy) which inhibits all AdoMet dependent methyltransferases and therefore must be efficiently eliminated. In mammalian cells AdoHcy is metabolized exclusively by AdoHcy hydrolase[2,3], producing adenosine (Ado), which regulates various cardiovascular and central neurological functions, and L-homocysteine, which has been implicated in causing vascular disease. Thus AdoHcy hydrolase is an essential enzyme playing a key role in regulating transmethylation and the level of two biologically active molecules and deletion of the gene is associated with embryo lethality in mice[4].

The mammalian AdoHcy enzyme is a homotetramer of ~48,000 M_r subunits, each of which contains one mole of NAD^+. The reaction mechanism proposed by Palmer and Abeles involves a cycle of reciprocal oxidation-reduction of substrate and NAD cofactor, the latter of which remains tightly enzyme-associated[5]. AdoHcy hydrolase also forms a tight complex with Ado while 2'-deoxyadenosine (2dAdo) causes type-I mechanism-based inactivation of the enzyme[6,7]. Reduction in AdoHcy hydrolase activity due to binding of either Ado or 2dAdo has been implicated in causing severe combined immunodeficiency (SCID) in patients with inherited adenosine deaminase deficiency[6–9]. Numerous Ado analogs that inhibit or inactivate AdoHcy hydrolase also have antiviral or immunosuppressive activity[10–12]. The X-ray structure determination of human AdoHcy hydrolase was undertaken to better understand the mechanism of catalysis, inhibition and inactivation, and to permit the design of more potent and selective mechanism-based inhibitors.

Solution of selenium substructure

Human AdoHcy hydrolase complexed with NADH and the type I mechanism-based inhibitor (1'R, 2'S, 3'R)-9-(2', 3'-dihydroxycyclopentan-1'-yl) adenine (DHCaA) was crystallized, and preliminary data analysis showed the asymmetric unit to contain a dimer[13]. Since a search for heavy atom derivatives was

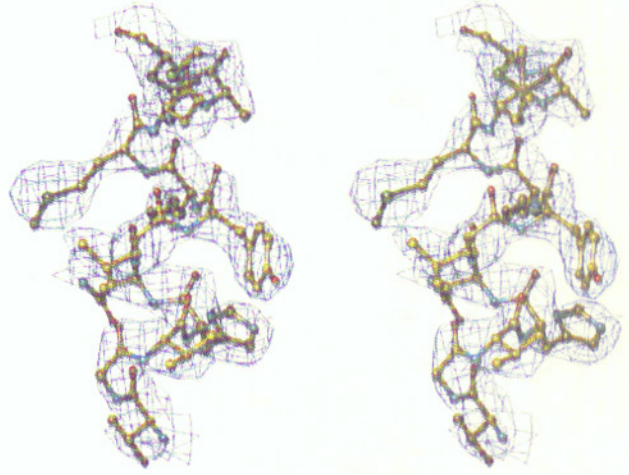

Fig. 1 Stereo pair of the initial electron density map after solvent flattening. The position of the refined coordinates (residues A159–A170) have been shown for comparison. The map is contoured at 1σ. Figure prepared using Turbo-Frodo. (Roussel, A. & Cambillau, C.; LCCMB, Biographics, Marseille, 1992).

[1]Structural Biology and Biochemistry, Research Institute, Hospital for Sick Children, 555 University Avenue, Toronto, M5G 1X8, Ontario, Canada. [2]Departments of Biochemistry and Pharmaceutical Chemistry, University of Kansas, Lawrence, Kansas 66045, USA. [3]Present address: Tanabe Research Laboratories USA Inc., 4540 Towne Center Court, San Diego, California 92121, USA. [4]Departments of Medicine and Biochemistry, Duke University Medical Center, Durham, North Carolina 77071, USA. [5]Hauptman-Woodward Medical Research Institute, 73 High Street, Buffalo, New York 14203, USA. [6]Roswell Park Cancer Institute, Elm and Carlton Streets, Buffalo, New York 14263, USA. [7]Department of Biochemistry, Faculty of Medicine, University of Toronto, Medical Sciences Building, Toronto, M5S 1A8, Ontario, Canada.

Correspondence should be addressed to P.L.H. *email: howell@sickkids.on.ca*

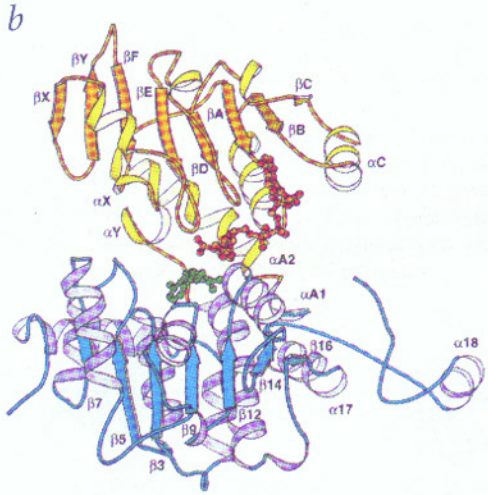

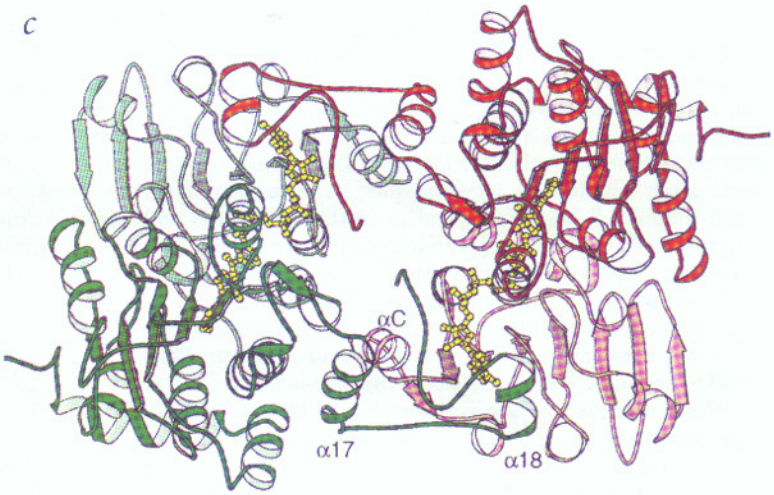

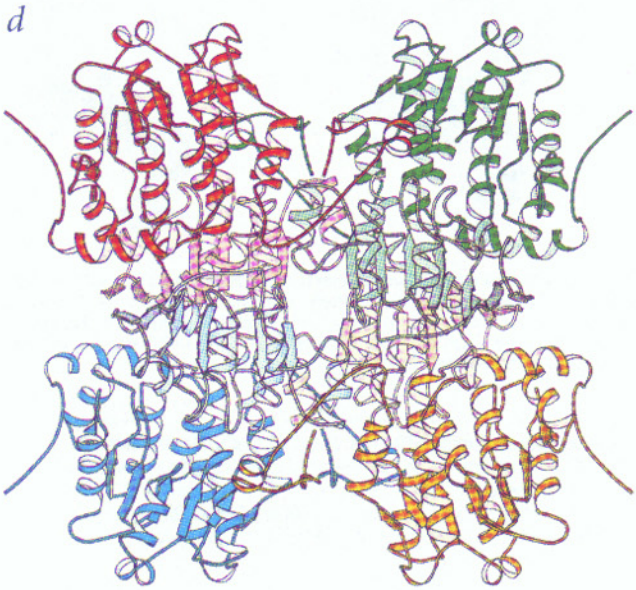

Fig. 2 Schematic representation of the topology of the AdoHcy hydrolase. ***a***, Stereo diagram of the Cα trace of AdoHcy monomer with NADH and inhibitor. Amino acid residues are labeled every 20 residues. ***b***, The AdoHcy monomer. The NAD binding domain is represented in yellow/orange and the catalytic domain in blue/purple. The position of both the DHCeA inhibitor (green) and the NADH molecule (red) are shown. For clarity only the β-sheet and selected α-helical secondary structural elements are labeled. ***c***, Dimer representation. In (*c*) and (*d*) each monomer is represented by two different shades of the same colour, the NAD binding domain is represented by the lighter shade in each case. The diagram highlights the interaction of the C-terminal helices, α17 and α18 with the NAD binding domain of the second monomer (especially helix αC). The NAD and inhibitor molecules are represented in yellow. ***d***, Tetramer representation. Although a dimer is present in the crystallographic asymmetric unit, AdoHcy hydrolase is catalytically active as a tetramer. This diagram has been drawn at 90° to the orientation presented in (*b*). The dimer–dimer interactions occur predominantly between the NAD binding domains. Figure prepared using MOLSCRIPT[51].

unsuccessful, the protein was expressed in the presence of selenomethionine prior to performing a multiwavelength anomalous diffraction (MAD) experiment[14]. Although the sequence of AdoHcy hydrolase would be expected to contain 16 methionine residues in 432 amino acids, results from sequence analysis determined that the N-terminal methionine had been cleaved. Therefore, the NADH/(1'R, 2'S, 3'R)-9-(2', 3'-dihydroxycyclopent-4'-enyl) adenine (DHCeA)[15] complex of the selenomethionyl-incorporated protein, crystallized under similar conditions to that of the native protein complexed to DHCaA, should contain 30 selenium atoms in the asymmetric unit. A MAD experiment carried out at three wavelengths provided data to 2.8 Å resolution with statistics listed in Table 1. Searches of conventional Patterson maps calculated with coefficients $||F^+| - |F^-||^2$, $||E^+| - |E^-||^2$, $||F\lambda_1| - |F\lambda_3||^2$ or normalized $|F_a|^2$ failed to provide a solution.

While MAD phasing has had many successes in recent years, considerable difficulty has been encountered in the determination of the anomalous scattering substructure from the resulting $|F_a|$'s when the number of such atoms exceeds twenty. However, the use of *Snb* v2.0[16] (C.M. Weeks, personal commu-

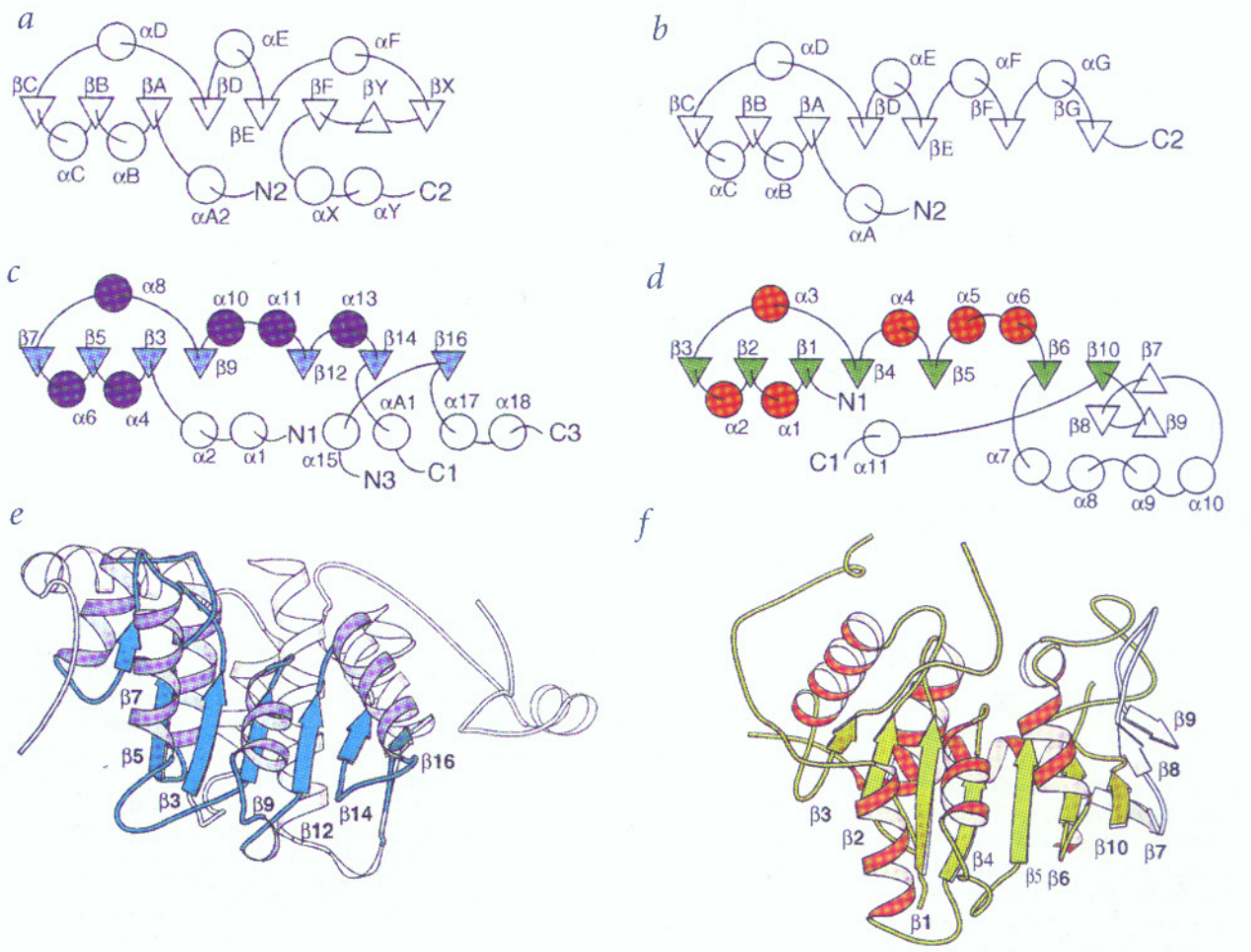

Fig. 3 Schematic representations showing the similarities of the topologies of the NAD binding domains of ***a***, AdoHcy hydrolase and ***b***, formate dehydrogenase, and (***c***,***e***) the catalytic domain of AdoHcy hydrolase and (***d***,***f***) inosine-uridine nucleoside N-ribohydrolase. In (*c–f*) the regions of secondary structure in common between the catalytic domain of AdoHcy hydrolase and inosine-uridine N-ribohydrolase have been represented in color. In (*a*) and (c) the N- and C-termini are numbered sequentially, that is N1 is the N-terminus of the protein, and C1 is the end of the first part of the catalytic domain and is connected to N2 in the NAD binding domain, and so forth. The secondary structural elements in AdoHcy hydrolase were defined using PROMOTIF[52] and are as follows: α1, residues 12–26; α2, 30–39; β3, 49–53; α4, 58–69; β5, 73–77; α6, 86–94; β7, 99–101; α8, 107–118; β9, 127–130; α10, 134–142; α11, 147–149; β12, 152–155; α13, 158–168; β14, 177–179; αA1, 184–187; αA2, 190–207; βA, 215–219; αB, 223–234; βB, 238–242; αC, 246–254; βC, 258–260; αD, 262–265; βD, 271–274; αE, 284–287; βE, 294–298; αF, 308–314; βX, 315–322; βY, 325–329; βF, 335–339; αX, 340–342; αY, 345–349; α15, 355–374; β16, 383–385; α17, 388–397; α18, 411–416. Panels (*a–d*) adapted from the program TOPS[53]. Panels (*e*, *f*) prepared using MOLSCRIPT[51].

nication) in conjunction with anomalous difference E-magnitudes (diffE's)[17] from peak data (Table 1), provided the positions of all 30 selenium atoms present in the asymmetric unit in eight of 350 trial structures (see Methods) and the edge wavelength data provided the positions of 24 selenium atoms in four of 500 trials. This represents the largest selenomethionyl substructure solved to date from a single wavelength or from a MAD analysis of protein data in the absence of any previously determined phases. The selenium atomic positions were refined treating the data as a special case of MIR[18] using the PHASES package[19]. The resulting solvent flattened map shown in Fig. 1 allowed the entire protein and NADH cofactor to be built. The structure was refined with maximum likelihood torsion angle dynamics refinement using the program CNS[20].

Monomer structure

The AdoHcy hydrolase monomer is folded into a two-domain structure reminiscent of NAD-dependent dehydrogenases (Fig. 2*a*,*b*). The coenzyme-binding domain and catalytic domains both exhibit a core of parallel α/β structure with the NAD and substrate binding sites located in the cleft between the two domains. Comparison of the monomer with the database[21] showed highest structural homology with formate dehydrogenase (FDH)[22]. The root-mean-square (r.m.s.) difference between 142 structurally homologous Cα atom positions was 2.4 Å. The coenzyme binding domain, residues 193–346, is formed from six strands of parallel β-sheet denoted βC, βB, βA, βD, βE, βF according to NAD-dependent dehydrogenase nomenclature[23] in the topology +1x+1x-3x-1x-3x+1+1 (ref. 24). The nomenclature refers to the connectivity of each β-strand within the β-sheet structure starting from the N-terminal strand, βA. Each connection is named according to how many strands it moves over in the sheet and in which direction, with an 'x' added for crossover connections. Thus +1 is a hairpin turn and +1x is a crossover connection between nearest neighbors. A comparison of the topology of the coenzyme binding domains of these proteins is illustrated in Fig. 3*a*,*b*. The AdoHcy hydrolase cofactor binding domain differs from

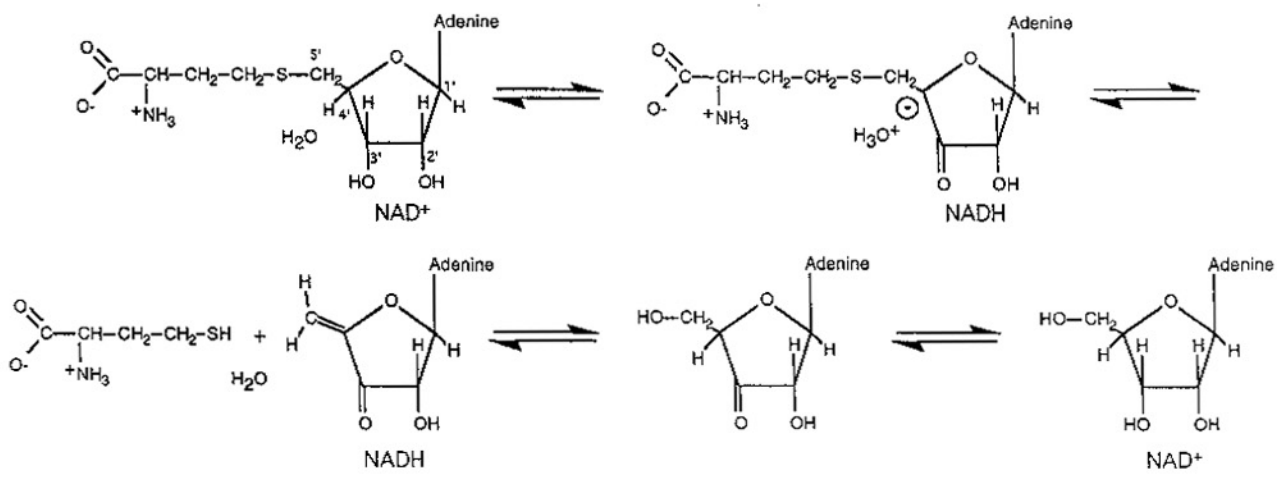

Fig. 4 The mechanism of action of AdoHcy hydrolase adapted from Palmer and Abeles5. Figure prepared using ChemDraw (Rubenstein, S.; Cambridge Scientific Computing Inc, Cambridge, Massachusetts 02139 USA, 1987).

the canonical NAD binding topology of +1x+1x-3x-1x-1x (ref. 25) with an excursion of two strands of antiparallel sheet, βX and βY, inserted between αF and βF which extend the parallel α/β core adjacent to βF. Although deviations from classic NAD-binding structure are known[22,26–29], the differences observed in the AdoHcy hydrolase fold appear to be unique and important to the catalytic mechanism of this enzyme. Where strand βF normally packs tightly against βE, βF in AdoHcy hydrolase is pulled away mid-strand and stabilized by hydrogen bonds to the first antiparallel strand βY, creating a gap that is filled by the short 3_{10}-helix, αX. This helix contains residues thought to be involved in interactions with the homocysteinyl tail of the AdoHcy substrate. Helix αY, which immediately follows αX, is involved in cofactor binding. Furthermore, helix αY, along with helices αA1 and αA2, form the transitional segments between the coenzyme binding and catalytic domains.

The catalytic domain, residues 1–190 and 355–432, also exhibits the dinucleotide binding fold with the topology +1x+1x-3x-1x-1x-1x. This domain has striking structural similarity[21] with inosine-uridine nucleoside N-ribohydrolase (IUNH) from the parasite *Crithidia fasciculata*[30]. The r.m.s. difference between 91 Ca atom positions for the matching secondary structure elements is 2.18 Å (Fig. 3*c–f*). No significant amino acid sequence homology was detected from using the program GCG (Genetics Computer Group, Madison, Wisconsin 53711, 1995).

. In both the catalytic domain and in IUNH, an excursion from the core parallel sheet to form the second domain occurs after the sixth strand (b14, AdoHcy hydrolase; b6, IUNH). The second smaller domain in IUNH, consisting of helices a7–a10, is formed before the chain returns to complete two antiparallel strands and extend the core sheet. In AdoHcy hydrolase, the NAD-binding domain is formed before the protein chain returns to the catalytic domain to add one further parallel strand to the core sheet.

Novel mode of NAD binding

The crystallographic asymmetric unit contains two subunits of AdoHcy hydrolase that form the dimer illustrated in Fig. 2*c*. This dimer has a unique NAD-binding domain interface involving an interaction between helices α17 of one monomer and αC of the other, and between α18 of one monomer and residues at the adenine side of the NAD binding site in the other monomer. Unlike NAD-dependent dehyrogenases, where each cofactor is typically bound by one monomer exclusively, NAD binding to AdoHcy hydrolase requires contributions from both dimer subunits. Both Lys 426 and Tyr 430 of one monomer are involved in interactions with the NAD bound predominantly to the other monomer. Lys 426 Nζ forms hydrogen bonds to either of the sugar hydroxyls O 2' or O 3' at the nicotinamide end of the NAD cofactor. The Oη of Tyr 430 is also involved in a hydrogen bond with a phosphate oxygen on the adenine side of NADH. The intersubunit dependency for NAD binding in AdoHcy hydrolase is evidenced by site-directed mutagenesis studies that highlight the importance of Lys 426 to enzyme activity and indeed to maintaining the tetrameric structure[31].

Otherwise, binding of the NAD cofactor is largely typical of NAD-dependent dehydrogenases. Interactions with NAD at the GXGXXG motif are through hydrogen bonds between Asp 223 N and pyrophosphate oxygens on either the nicotinamide or adenine sides of NAD as well as between Val 224 N and a pyrophosphate oxygen on the nicotinamide side of NAD. In AdoHcy hydrolase, Glu 243 performs the role of the highly conserved aspartate residue located in the NAD-dependent dehydrogenases approximately 20 residues C-terminal to the GXGXXG motif. This residue interacts with a ribose hydroxyl of the Ado moiety[25]. Helix αY, in addition to linking the cofactor-binding and catalytic domains, also forms hydrogen bonds to N7 and O7 of nicotinamide through Oδ1 of Asn 346.

Tetramer formation

Intersubunit interactions in FDH and the structurally similar glycerate dehydrogenase[32] (GDH) occur mainly through the αA helix of the coenzyme binding domain. FDH and GDH are dimeric and at the time of their structural solutions, constituted a new subfamily of NAD-dependent dehydrogenases. An identical intersubunit interaction is observed in AdoHcy hydrolase through helices αA1 and αA2 with a crystallographic symmetry-related monomer. This interaction forms the basis for AdoHcy hydrolase tetramer formation. Quaternary assembly also involves interactions between catalytic domains that are located on the periphery of the tetramer (Fig. 2*d*).

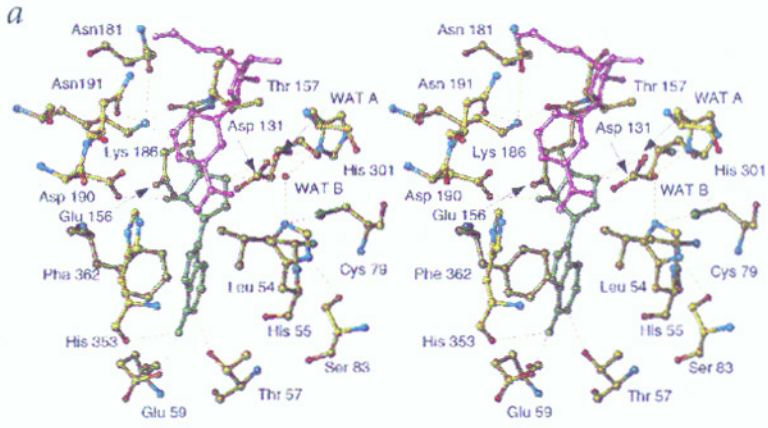

Fig. 5 ***a***, Stereo view of the inter-actions between AdoHcy hydrolase and the inhibitor, DHCeA (green). Part of the NADH molecule (pink) has been included for completeness. Panel prepared using Turbo-Frodo (Roussel, A. & Cambillau, C.; LCCMB, Biographics, Marseille, 1992). ***b***, Schematic diagram of the inter-actions between AdoHcy hydrolase and the inhibitor, DHCeA showing hydrogen bond distances. Panel prepared using ChemDraw (Rubenstein, S.; Cambridge Scientific Computing Inc, Cambridge, MA 02139 USA, 1987).

Catalytic mechanism

The catalytic mechanism of AdoHcy hydrolysis has been described by Palmer and Abeles[5] (Fig. 4). The first step involves oxidation of the substrate at the 3'-OH group by enzyme-bound NAD^+ to form NADH and the 3'-keto AdoHcy intermediate. The C4'-proton is rendered more acidic and is abstracted by a base in the second step. This is followed by elimination of homocysteine to form 3'-keto-4',5'-didehydro-5'-deoxy-Ado. Water is then added across the double bond in a Michael-type addition and the 3'-keto-4'-dehydro-Ado is reprotonated and reduced by NADH to yield Ado. The most potent inhibitors of AdoHcy hydrolase are Ado analogs that are oxidized by enzyme-bound NAD^+ to give the inactive enzyme-bound NADH. This type of inhibitor has been defined as a type I mechanism-based inhibitor[33]. Type II mechanism based inhibitors are defined as those that are activated by the enzyme in the first step and irreversibly inactivate the enzyme subsequently through covalent modification. The complexed inhibitor DHCeA is a type I mechanism based inhibitor that is oxidized by NAD^+ to form the keto intermediate.

The enzyme active site is illustrated in Fig. 5. It is interesting to note that although the structure of IUNH was solved in the absence of substrate or inhibitor, the proposed active site is very close to the location of the inhibitor found in the AdoHcy hydrolase complex. The function of IUNH is to catalyze the hydrolysis of the N-ribosidic bond in the formation of purine and ribose. This reaction is analogous to that which occurs when AdoHcy hydrolase is inhibited by 2dAdo[34]. AdoHcy hydrolase catalyses the breakdown of the 2dAdo to ribose and adenine by two different mechanisms, only one of which involves oxidation to 3'-keto-2'-deoxyadenosine[34].

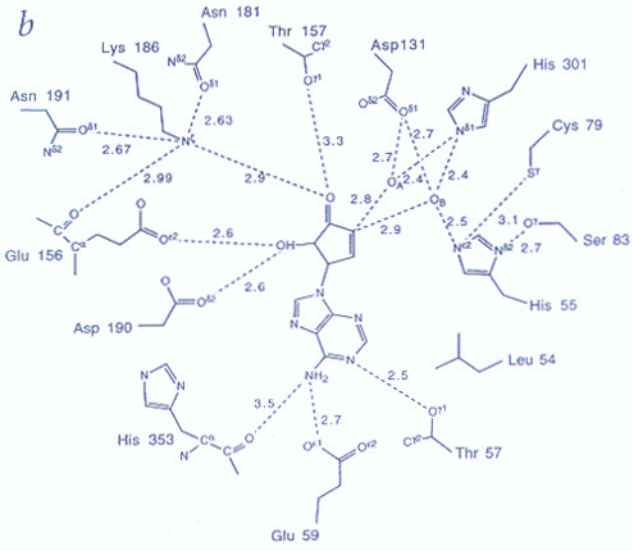

The nicotinamide and cyclopentenyl ring of the oxidized inhibitor stack suggesting a hydride transfer of C 3'H to the C4 of NAD^+ with A-face stereochemistry. The side chain of Lys 186 is rendered more nucleophilic as a result of hydrogen bonds through Nζ to the carbonyl oxygen of Glu 156 and to the side chains of Asn 191 and Asn 181 and is the likely acceptor of the O 3'-proton. The role of proton abstraction from C4' is assigned to a water molecule (WAT A, WAT B) located at a distance of 2.9 Å from C4' in site A (2.8 Å in site B). Evidence for solvent exchange of C4'H with [^{3}H] H_2O is documented by Palmer and Abeles[5]

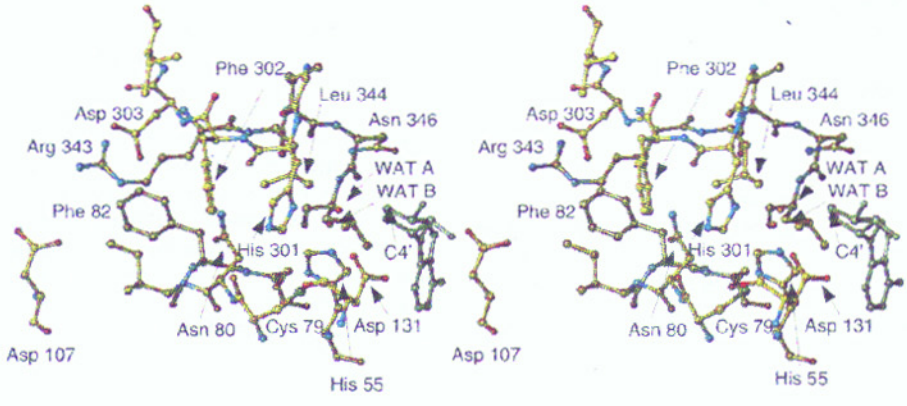

Fig. 6 Stereo view of the active site tunnel highlighting the locations of His 301, Phe 302, Asp 303 and Arg 343. The orientation of the inhibitor (green) and both water molecules (WAT A and B) suggest that the homocysteinyl tail will lie right to left across the figure as described in the text. Figure prepared using Turbo-Frodo (Roussel, A. & Cambillau, C.; LCCMB, Biographics, Marseille, 1992).

Table 1 Data reduction and phasing statistics

Data Collection	Edge	Peak	Remote
Wavelength (Å)	0.9789	0.9784	0.95
f', f"	-9.52, 3.15	-7.35, 5.92	-3.81, 3.74
Resolution (Å)	2.8	2.8	2.8
Total data	345,476	347,188	350,530
Unique data	50,276	50,469	50,613
Redundancy	6.9	6.9	6.9
Overall completeness 50–2.8Å (2.9–2.8Å)	99.3 (97.7)	99.4 (97.8)	99.5 (99.5)
$F^2 > 3\sigma(F^2)$	93.1(82.3)	91.8(79.9)	91.3(80.2)
R_{merge} (%)	6.8	7.1	7.4
Average $F^2/\sigma(F^2)$	11.84	10.43	10.49
B_{iso} (Å^2) from program Levy[45]	18.7	18.6	18.8
No. of reflections which passed diffE tests[1]	3,557	974	
No. of diffE's used	600	600	
No. of invariants generated	6,000	6,000	
Phasing			
Phasing power (anomalous)	3.67	5.19	2.83
Phasing power (isomorphous)		2.04	2.21
FOM before solvent flattening	0.824		
FOM after solvent flattening	0.909		

[1]Difference E-magnitudes were obtained through the use of the program diffE and subjected to the following criteria for inclusion in input into *SnB* v2.0: (i) minimum of $|E^+|/\sigma|E^+|$ or $|E^-|/\sigma|E^-| > 3.0$; (ii) $(||E^+|-|E^-||/[\sigma^2(E^+)+\sigma^2(E^-)]^{1/2} > 1.0$; and (iii) renormalized diffE's (diffE = $\{\Sigma[(f+f')^2 + f''^2]\ ||E^+|-|E^-||\}^{1/2}/2q(\Sigma f''^2)^{1/2}$, where q is a least-squares fitted normalization function of $\sin\Theta/\lambda$ such that $<\text{diffE}^2> = 1.0$) were greater than 3σ(diffE).

and no protein residue is in position to act as an abstractor in the inhibitor complex. No non-crystallographic symmetry (NCS) restraints were imposed on the solvent sites during refinement and the location of the water molecule is slightly different in the two NCS-related active sites; both water positions are indicated in Fig. 5. In site A, only His 301 (2.4 Å) and Asp 131 (2.7 Å) are involved in hydrogen bonds with the water molecule. In site B, the water molecule is hydrogen bonded to His 55 (2.5 Å), Asp 131 (2.7 Å), and His 301 (2.4 Å).

The short hydrogen bonding distances found in this inhibitor complex may be indicative of the presence of low-barrier hydrogen bonds[35] as both His 55 and His 301 are implicated in the catalytic mechanism. A change in the side chain conformation of His 301 would be required during natural substrate binding to avoid a steric clash. Therefore, His 301 would not be available to interact with the water molecule until after elimination of homocysteine. Although the existence of a hydrogen bond with His 301 likely perturbs the position of the active site water from its exact location during AdoHcy C4' proton abstraction, this water molecule remains the only plausible candidate to accept the proton abstracted from C4'.

Based on the current inhibitor complex and evidence from chemical modification studies, the following mechanism is proposed for AdoHcy hydrolase (Fig. 4). The nucleophilicity of the active site water is enhanced by hydrogen bonds with Asp 131 and His 55 and is thus activated to abstract the C4' proton. His 55 may in turn be rendered more nucleophilic by interactions with Cys 79 Sγ. Chemical modification studies implicate the indirect participation of an unidentified amino acid residue[36] and Cys 79[37,38] in the proton abstraction step of the catalytic mechanism since modification of Cys 79 by 5'-[p-fluorosulfonyl)benzoyl]adenosine reduced the rate of C4' proton exchange to 9% of that of the native protein[38]. After proton abstraction in the natural substrate and elimination of cleaved homocysteine, His 301 is relieved of its steric restriction and is free to participate in an interaction with the active site water molecule similar to that visualized in the present structure.

Chemical modification of histidine by diethylpyrocarbonate showed that activity is eliminated by the modification of a single histidine residue[39]. Oxidation of the substrate and abstraction of the C4' proton occur with the modified protein, but the subsequent Michael-type addition of water to the double bond formed after elimination of homocysteine was inhibited. Of the two histidines present in the active site, it is likely that this chemical modification involves only His 301. The eliminated homocysteinyl moiety is protonated by the catalytic water molecule. With the elimination of homocysteine, the side chain of His 301 is free to participate in an activation of the catalytic water molecule which then adds to the 4'-5' double bond. The reduction of 3'-ketoadenosine by NADH completes the last mechanistic step. This inhibitor structure provides no insight into how the protein catalyzes the breakdown of 2dAdo.

Table 2 Refinement statistics

Refinement		
Number of reflections	49,579	
R-factor (R_{free})[1]	22.16% (24.27%)	
R.m.s.d. bonds (Å)	0.008	
R.m.s.d. angles (°)	1.68	
R.m.s.d. NCS (Å) (4,087 atoms)	0.28	
No. of atoms (average B value (Å^2))	monomer A	monomer B
Protein[2]	3,336 (17.51)	3,330 (26.04)
NADH	44 (16.16)	44 (18.66)
Inhibitor	17 (15.48)	17 (43.75)

[1]R-factor reported for all data with no σ cutoff. Data prepared with the program scalepack2xplor[54].
[2]Monomer A, residues 2–432; monomer B, residues 3–432.

The active site in this complex is remarkably sequestered from solvent. The path of entry of the substrate from the protein's exterior is most likely through a tunnel that may be more open in the absence of inhibitor than in the present structure. The two sides of the tunnel are formed by the catalytic and nucleotide binding domains respectively. In this inhibitor complex, the side chain of Phe 302 obstructs the tunnel (Fig. 6) and it is likely that this residue is involved in hydrophobic interactions with the aliphatic chain of the homocysteine moiety during reaction with AdoHcy. The side

chains of residues Arg 343 and Asp 303 are located at the entrance to the tunnel and are proposed to be involved in hydrogen bonds or salt bridges to the amino and carboxyl groups of AdoHcy. Arg 343 is located in the 3_{10}-helix, αX, a helix not present in NAD-dependent dehydrogenases.

The deviation of the fold of AdoHcy hydrolase from that of classic dinucleotide binding is therefore important and required for substrate binding. The αA1 and αA2 helices appear to have arisen from a kink in an otherwise continuous αA helix present in the structures of FDH and GlDH and it is possible that this kink is the result of a hinge motion in which the two domains close around the inhibitor in the active site of this structure. Access to the active site through an opening and closing of the tunnel is also aided by the general distribution of the catalytic domains around the periphery of the tetramer (Fig. 2*d*) as their motion is relatively uninhibited by intersubunit interactions. Although not conclusive, fluorescence studies seem to support this hypothesis as a 10% change in fluorescence, attributed to an alteration in tertiary structure[40], is observed on inhibitor binding.

Summary

In summary, the AdoHcy hydrolase structure shows a deviation from the nucleotide binding fold that is essential for catalytic activity. The proposed mechanism implicates a dual role for an active site water, not only in the abstraction of the C4'proton but also in the addition of water across a double bond in the Michael-type addition. The identification of a water molecule as the catalytic base was not expected and will have significant consequences for the design of other mechanism based inhibitors. Finally, given the ease with which this structure was solved, the use of *Snb* in conjunction with diffE's should prove to be applicable to larger numbers of selenium atoms than are currently considered practical.

Methods

Incorporation of Se-methionine and crystallization. In order to produce the selenomethionyl-incorporated (Se-Met) AdoHcy hydrolase, the pporkcd20 plasmid containing the gene encoding the protein was transformed into the Met auxotrophic *E. coli* strain B834 (DE3). The transformed bacteria were grown in 1 l of M9 medium supplemented with 0.06 g of Se-Met[41]. Cells were harvested 15 h after induction with IPTG and the protein was purified following the same procedure as described[42] except that all buffers used for Se-Met protein purification contained 5 mM DTT. The percentage of Se-Met incorporation was examined by amino acid analysis and was found to be approximately 90%.

Data collection and reduction. Crystals with C222 space group symmetry had dimensions a = 91.93, b = 168.02 and c = 137.77 Å. Multiwavelength anomalous diffraction (MAD) data were collected from a single crystal at 100 K to 2.8 Å resolution using a Brandeis CCD detector at beamline X12-C of the National Synchrotron Light Source, Brookhaven National Laboratory. The data were collected using inverse beam geometry with each set of data measured as a single wedge of data. The data were initially processed (Table 1) using the programs DENZO and SCALEPACK[43], treating Bijvoet pairs as independent measurements. The data at the three wavelengths were processed independently using the DREAR program package[44], applying Bayesian processing[45], local scaling[46] and generating E-magnitudes from a Wilson analysis. Difference E-magnitudes were generated using the program diffE. A total of 6,000 triple invariants were generated from the largest 600 diffE magnitudes from the peak data using *Snb* v2.0. Each of 350 trials contained 32 random atoms, and each trial structure was subjected to 34 cycles of phase refinement. The trace of the minimal function, R_{min}, clearly identified the eight correct solutions. Allowing for all possible origins and two enantiomorphs, the positions of all 30 selenium atoms in the eight solutions were identical.

Model refinement. The initial model was built from experimental maps using the program O[47]. The orientation of the NCS symmetry axis was calculated from the averaged experimental map[48] and applied to coordinates of monomer A to generate the dimer. Initial refinement was performed using the remote wavelength data set with maximum likelihood torsion angle dynamics[16] incorporating the experimental phases as Hendrickson-Lattman distributions within the program CNS. All anomalous data between 50 and 2.8 Å resolution were included during refinement with a bulk solvent correction applied. Different weights for symmetry restraints of NCS related monomers were tested and applied to minimize R_{free}[49]. Each round of refinement was alternated with a round of manual refitting. Individual B-factor refinement was carried out after the second round of refinement as justified by the reduction of R_{free}. The B-factors for the inhibitor molecules indicate that the inhibitor in monomer B may only be present at partial occupancy. A total of 46 water molecules were added and refined using maximum likelihood Cartesian dynamics with the program CNS. A total of five rounds of refinement and rebuilding resulted in a model with all ϕ and ψ values in allowed regions of the Ramachandran plot and with 83% in the most favourable regions according to the program PROCHECK[50]. With the exception of Ser 2 in monomer B for which insufficient density was present, all residues and their side chains have been built into clear well defined density.

Coordinates. The coordinates and structure factors have been deposited in the Brookhaven Protein Data Bank (accession number 1A7A).

Acknowledgments

This work was supported in part by N.I.H. grants to R.T.B., P.L.H. and G.D.S. The authors thank X. Yang for help with protein purification, B. Sweet for help with data collection, C. Weeks for access to *Snb* v2.0 prior to its general release, and P. Adams and A. Brünger for help with and access to CNS prior to its general release.

Received 28 January, 1998; accepted 18 March, 1998.

1. Borchardt, R.T., Creveling, C.R. & Ueland, P.M. Biological methylation and drug design — Experimental and clinical roles of S-adenosylmethione (Humana Press, Clifton, NJ, 1986).
2. de la Haba, G. & Cantoni, G. The enzymatic synthesis of *S*-adenosyl-L-homocysteine from adenosine and homocysteine. *J. Biol. Chem.* **234**, 603–608 (1959).
3. Ueland, P.M. Pharmacological and biochemical aspects of S-adenosylhomocysteine and S-adenosylhomocysteine hydrolase. *Pharmacol. Rev.* **34**, 223–253 (1982).
4. Miller, M.W. *et al.* The mouse lethal *nonagouti* (*Ax*) mutation deletes the *S-adenosylhomocysteine hydrolase* (*Ahcy*) gene. *EMBO J* **13**, 1806–1816 (1994).
5. Palmer, J.L. & Abeles, R.H. The mechanism of action of *S*-adenosylhomocysteinase. *J. Biol. Chem.* **254**, 1217–1226 (1979).
6. Hershfield, M.S., Kredich, N.M. S-adenosylhomocysteine hydrolase is an adenosine-binding protein: a target for adenosine toxicity. *Science* **202**, 757–760 (1978).
7. Hershfield, M.S. Apparent suicide inactivation of human lymphoblast S-adenosylhomocysteine hydrolase by 2'-deoxyadenosine and adenine arabinoside: A basis for direct toxic effects of analogs of adenosine. **254**, 22–25 (1979).
8. Kredich, N.M. & Martin, D.W., Jr. Role of S-adenosylhomocysteine in adenosinemediated toxicity in cultured mouse T lymphoma cells. *Cell* **12**, 931–938 (1977).
9. Hershfield, M.S., Kredich, N.M., Ownby, D.R., Ownby, H. & Buckley, R. In vivo inactivation of erythrocyte S-adenosylhomocysteine hydrolase by 2'-deoxyadenosine in adenosine deaminase-deficient patients. *J. Clin. Invest.* **63**, 807–811 (1979).
10. Wolfe, M.S., Borchardt, R.T. S-adenosyl-L-homocysteine hydrolase as a target for antiviral chemotherapy. *J. Med. Chem.* **34**, 1521–1530 (1991).
11. Bitonti, A.J., Baumann, R.J., Jarvi, E.T., McCarthy, J.R. & McCann, P.P. Antimalarial activity of a 4',5'-unsaturated 5'-fluoroadenosine mechanism-based inhibitor of S-adenosyl-L-homocysteine hydrolase. *Biochem. Pharmacol.* **40**, 601–606 (1990).
12. Wolos, J.A., Frondorf, K.A. & Esser, R.E. Immunosuppression mediated by an inhibitor of S-adenosyl-L-homocysteine hydrolase. Prevention and treatment of collagen-induced arthritis. *J. Immunol.* **151**, 526–534 (1993).
13. Turner, M.A. *et al.* Crystallization and preliminary X-ray analysis of human placental S-adenosylhomocysteine hydrolase. *Acta Crystallogr.* **D53**, 339–341 (1997).
14. Hendrickson, W.A. Determination of macromolecular structures from anomalous diffraction of synchrotron radiation. *Science* **254**, 51–58 (1991).
15. Ault-Riche, D.B. *et al.* Effects of 4'-modified analogs of aristeromycin on the metabolism of S-adenosyl-L-homocysteine in murine L929 cells. *Mol. Pharmacol.* **43**, 989–997 (1993).
16. Miller, R., Gallo, S.M., Khalak, H.G. & Weeks, C.M. *Snb*: Crystal structure determination via Shake-and-Bake. *J. Appl. Crystallogr.* **27**, 613–621 (1994).
17. Smith, G.D., Nagar, B., Rini, J.M., Hauptman, H.A., Blessing, R.H. The use of *Snb* to determine an anomalous scattering substructure. *Acta Cryst.*, **in the press** (1998).
18. Ramakrishnan, V. & Biou, V. Treatment of multiwavelength anomalous diffraction data as a special case of multiple isomorphous replacement. *Meths Enz.* **76**, 538–557 (1997).
19. Furey, W. & Swaninathan, S. PHASES-95: A program for processing and analyzing diffraction data from macromolecules in *Methods in Enzymology* (eds. Carter, C.W. & Sweet, R.M.) 590–633 (Academic Press, New York, 1997).
20. Brünger, A.T. *et al.* Crystallography and NMR System (CNS): A new software system for macromolecular structure determination. *Acta Crystallogr. D*, submitted (1998).
21. Kleijwegt, G.J. & Jones, T.A. Detecting folding motifs and similarities in protein structures. *Meths Enz.* **277**, 525–545 (1997).
22. Lamzin, V.S. *et al.* Crystal structure of NAD-dependent formate dehydrogenase. *Eur. J. Biochem.* **206**, 441–452 (1992).
23. Rossman, M.J., Liljas, A., Branden, C.-I. & Banaszak, L.J. In *The Enzymes* (ed. Boyer, P.D.) 61–102 (Academic Press, New York; 1975).
24. Richardson, J.S. The anatomy and taxonomy of protein structure. *Adv. Protein Chem.* **34**, 167–339 (1981).
25. Lesk, A.M. NAD-binding domains of dehydrogenases. *Curr. Opin. Struct. Biol.* **5**, 775–783 (1995).
26. Buehner, M., Ford, G.C., Moras, D., Olsen, K.W. & Rossmann, M.G. D-Glyceraldehyde-3-phosphate dehydrogenase: three-dimensional structure and evolutionary significance. *Proc. Natl. Acad. Sci. USA* **70**, 3052–3054 (1973).
27. Philips, C., Gover, S. & Adams, M.J. Structure of 6-phosphogluconate dehydrogenase refined at 2Å resolution. *Acta Crystallogr.* **D51**, 290–307 (1995).
28. Ghosh, D. *et al.* Three-dimensional structure of holo 3α,20β–hydroxysteroid dehydrogenase: a member of a short-chain dehydrogenase family. *Proc. Natl. Acad. Sci. USA* **88**, 10064–10068 (1991).
29. Varughese, K.I., Skinner, M.M., Whiteley, J.M., Matthews, D.A. & Xuong, N.H. Crystal structure of rat liver dihydropteridine reductase. *Proc. Natl. Acad. Sci. USA* **89**, 6080–6084 (1992).
30. Degano, M., Gopaul, D.N., Scapin, G., Schramm, V.L. & Sacchettini, J.C. Three-dimensional structure of the inosine-uridine nucleoside N-ribohydrolase from *Crithidia fasciculata*. *Biochemistry* **35**, 5971–5981 (1996).
31. Ault-Riche, D.B., Yuan, C.S. & Borchardt, R.T. A single mutation at lysine 426 of human placental S-adenosylhomocysteine hydrolase inactivates the enzyme. *J. Biol. Chem.* **269**, 31472–31478 (1994).
32. Goldberg, J.D., Yoshida, T. & Brick, P. Crystal structure of a NAD-dependent D-glycerate dehydrogenase at 2.4 Å resolution. *J. Mol. Biol.* **236**, 1123–1140 (1994).
33. Yuan, C.-S., Liu, S., Wnuk, S.F., Robins, M.J., Borchardt, R.T. Design and synthesis of S-Adenosylhomocysteine hydrolase inhibitors as broad-spectrum antiviral agents. *Adv. Antiviral Drug Des.* **2**, 41–88 (1996).
34. Abeles, R.H., Fish, S. & Lapinskas, B. *S*-Adenosylhomocysteinase: Mechanism of inactivation by 2'-deoxyadenosine and interaction with other nucleosides. *Biochemistry* **21**, 5557–5562 (1982).
35. Cleland, W.W. & Kreevoy, M.M. Low-barrier hydrogen bonds and enzymic catalysis. *Science* **264**, 1887–1890 (1994).
36. Takata, Y., Tomoharu, G. & Fujioka, M. Chemical modification of *S*-adenosylhomocysteinase by a water-soluble carbodiimide. *Arch. Biochem. Biophys.* **240**, 827–835 (1985).
37. Gomi, T., Ogawa, H. & Fujioka, M. *S*-adenosylhomocysteinase from rat liver. Amino acid sequences of the peptides containing active site cysteine residues modified by treatment with 5'-p-fluorosulfonylbenzoyladenosine. *J. Biol. Chem.* **261**, 13422–13425 (1986).
38. Takata, Y. & Fujioka, M. 5'-[p-(Fluorosulfonyl)benzoyl] adenosine-mediated inactivation of *S*-adenosylhomocysteinase. *Biochemistry* **23**, 4357–4362 (1984).
39. Gomi, T. & Fujioka, M. Evidence for an essential histidine residue in *S*-adenosylhomocysteinase from rat liver. *Biochemistry* **22**, 137–143 (1983).
40. Yuan, C.-S., Yeh, J., Squier, T.C., Rawitch, A. & Borchardt, R.T. Ligand-dependent changes in intrinsic fluorescence of *S*-adenosylhomocysteine hydrolase: implications for the mechanism of inhibitor-induced inhibition. *Biochemistry* **32**, 10414–10422 (1993).
41. Doublié, S., Carter, C.W. in *Crystallization of nucleic acids and proteins: a practical approach* (eds Ducruix, A. & Giegé, R.) 311–317 (Oxford University Press, New York; 1992).
42. Yuan, C.S., Wnuk, S.F., Liu, S., Robins, M.J. & Borchardt, R.T. (E)-5',6'-didehydro-6'-deoxy-6'-fluorohomoadenosine: a substrate that measures the hydrolytic activity ofS-adenosylhomocysteine hydrolase. *Biochemistry* **33**, 12305–12311 (1994).
43. Otwinowski, Z. & Minor, W. Processing of X-ray diffraction data collected in oscillation mode. *Meths Enz.* **276**, 307–326 (1997).
44. Blessing, R.H. Data reduction and error analysis for accurate single crystal diffraction intensities. *Crystallogr. Rev.* **1**, 3–58 (1987).
45. French, S. & Wilson, K. On the treatment of negative intensity observations. *Acta Crystallogr.* **A34**, 517–525 (1978).
46. Blessing, R.H. *J. Appl. Crystallogr.* **30**, 176–178 (1997).
47. Jones, T.A., Zou, J.Y., Cowan, S.W., Kjeldgaard, M. Improved methods for building protein models in electron density maps and the location of errors in these models. *Acta Crystallogr.* **A47**, 110–119 (1991).
48. Kleijwegt, G.J. & Jones, T.A. In *From first map to final model* (eds. Bailey, S., Hubbard, R. & Waller, D.) 59–66 (SERC Daresbury, Warrington; 1994).
49. Brünger, A.T. The free R value: a novel statistical quantity for assessing the accuracy of crystal structures. *Nature* **355**, 472–474 (1992).
50. Laskowski, R.A., MacArthur, M.W., Moss, D.S. & Thornton, J.M. PROCHECK: a program to check the stereochemical quality of protein structures. *J. Appl. Crystallogr.* **26**, 283–291 (1993).
51. Kraulis, P.J. MOLSCRIPT: A program to produce both detailed and schematic plots of protein structures. *J. Appl. Crystallogr.* **24**, 946–950 (1991).
52. Hutchinson, E.G. & Thornton, J.M. PROMOTIF—a program to identify and analyze structural motifs in proteins. *Protein Sci.* **5**, 212–220 (1996).
53. Flores, T.P., Moss, D.S. & Thornton, J.M. An algorithm for automatically generating protein topology cartoons. *Protein Engng.* **7**, 31–37 (1994).
54. Brünger, A.T. *XPLOR Version 3.1* (Yale University Press, New Haven, Connecticut; 1993).